Quantum Science and Technology



**LETTER** • **OPEN ACCESS**

# Quantum algorithm for polaritonic chemistry based on an exact ansatz

To cite this article: Samuel Warren *et al* 2025 *Quantum Sci. Technol.* **10** 02LT02

IOP Publishing Quantum Sci. Technol. 10 (2025) 02LT02 https://doi.org/10.1088/2058-9565/ad9fa5

Quantum Science and Technology



OPEN ACCESS

RECEIVED
17 September 2024

REVISED
11 December 2024

ACCEPTED FOR PUBLICATION
16 December 2024

PUBLISHED
28 January 2025



LETTER

# Quantum algorithm for polaritonic chemistry based on an exact ansatz

**Samuel Warren**[1], **Yuchen Wang**[1], **Carlos L Benavides-Riveros**[2,*] **and David A Mazziotti**[1,*]

[1] Department of Chemistry and The James Franck Institute, The University of Chicago, Chicago, IL 60637, United States of America
[2] Pitaevskii BEC Center, CNR-INO and Dipartimento di Fisica, Universitá di Trento, I-38123 Trento, Italy
* Authors to whom any correspondence should be addressed.

**E-mail:** cl.benavidesriveros@unitn.it and damazz@uchicago.edu

**Keywords:** polaritons, strong electron correlation, density matrix methods, contracted quantum eigensolver, mixed particles, wave function ansatz

## Abstract

Cavity-modified chemistry uses strong light-matter interactions to modify the electronic properties of molecules in order to enable new physical phenomena such as novel reaction pathways. As cavity chemistry often involves critical regions where configurations become nearly degenerate, the ability to treat multireference problems is crucial to understanding polaritonic systems. In this Letter, we show through the use of a unitary ansatz derived from the anti-Hermitian contracted Schrödinger equation that cavity-modified systems with strong correlation, such as the deformation of rectangular $H_4$ coupled to a cavity mode, can be solved efficiently and accurately on a quantum device. In contrast, while our quantum algorithm can be made formally exact, classical-computing methods as well as other quantum-computing algorithms often yield answers that are both quantitatively and qualitatively incorrect. Additionally, we demonstrate the current feasibility of the algorithm on near intermediate-scale quantum hardware by computing the dissociation curve of $H_2$ strongly coupled to a bosonic bath.

Polaritonic chemistry is a young discipline that exploits confined electromagnetic field modes to enable chemical processes that are not possible in bare materials [1–3]. It has been shown, for example, that polaritons can modify photochemical reaction rates [4, 5], transition rates between different spin multiplets [6] or charge transfer in chemical reactions [7, 8]. Hybridized light-matter states are also crucial for exploring quantum states of matter or quantum phase transitions [9, 10] and are central in the emergent field of cavity quantum materials [11, 12]. From a theoretical viewpoint, polaritonic systems exhibit an intrinsic strong multi-reference character [13] and require an equal quantum-mechanical treatment of both bosonic and fermionic statistics. It is thus no surprise that studying molecular polaritonic systems is a very demanding computational task.

Recently, quantum-computing methods for solving electronic structure problems have emerged as promising computational tools to combat the curse of dimensionality [14–16]. The most prominent algorithm proposed for use on noisy intermediate scale quantum (NISQ) devices is the variational quantum eigensolver (VQE), often using a unitary coupled cluster (UCC) ansatz [17]. These methods, however, tend to inherit some of the pitfalls of classical coupled cluster methods [18–20], namely, an inability to treat static correlation [21] and the need for truncation in the number of exponential operators [22]. In addition, the extension of the ansatz to arbitrary systems (e.g. where bosonic modes are present) is not always straightforward [23, 24]. In parallel, methods derived from the contracted Schrödinger equation (CSE) forming the set of algorithms known as the contracted quantum eigensolvers (CQE) have been shown to find exact ground and excited states for fermionic [25–27] and bosonic [28] systems with an ansatz whose underlying structure is universal. A subset of these algorithms focusing on the anti-Hermitian portion of the CSE, known as the ACSE, are particularly promising on NISQ devices [29].

Originally derived for fermionic systems [30–37], the CSE was recently extended to mixed Boson-Fermion systems [38]. The main result of that extension is an exact ansatz that can be implemented

directly on quantum devices to find eigenstates of arbitrary mixed-particle Hamiltonians. Remarkably, the CSE uniquely allows the ansatz to have the same degrees of freedom as the original many-body Hamiltonian (e.g. a purely two-body ansatz for the traditional electronic structure problem). Here, based on those previous results, we present a quantum algorithm for molecular polaritonic chemistry. We show that cavity-modified systems exhibiting strong quantum correlation, such as the deformation of rectangular $H_4$ coupled to a cavity mode, can be accurately solved by using the simple unitary ACSE ansatz. Additionally, to demonstrate the current feasibility of the algorithm, we compute the dissociation curve of molecular hydrogen coupled to a bosonic bath on NISQ hardware.

The Letter is structured as follows. First, we discuss how the ACSE naturally adapts to arbitrary quantum many-body systems. Next, we introduce the non-relativistic Pauli–Fierz Hamiltonian and discuss how our algorithm works for this problem as well as its favorable computational and measurement scaling on a quantum device. In the latter half of the paper, we will compare the results of the ACSE to quantum electrodynamics coupled cluster (QED-CC). We will also demonstrate the effectiveness of our ansatz on a real quantum device. Finally, we will discuss potential future directions and implications for our results.

*Theory*.— Before studying a polaritonic system, we review the fully general version of the CSE [32, 39] which can be used for arbitrary quantum many-body systems. We define a many-body $M$-term Hamiltonian:

$$\hat{H} = \sum_{\ell=1}^{M} f_\ell \hat{h}_\ell, \tag{1}$$

where $\{f_\ell\}$ is the set of Hamiltonian's parameters and $\hat{h}_\ell$ is a general many-body operator. The stationary state problem or the (time-independent) Schrödinger equation reads: $\hat{H}|\Psi_m\rangle = E_m|\Psi_m\rangle$. After multiplying on the left by $\langle\Psi_m|\hat{h}_\ell$, one obtains the CSE:

$$\langle\Psi_m|\hat{h}_\ell\left(\hat{H} - E_m\right)|\Psi_m\rangle = 0\,. \tag{2}$$

The equivalence of this equation and the standard Schrödinger equation can be proved by multiplying equation (2) by the parameter $f_\ell$ and summing the resulting expression over the indices $\ell$, which yields the energy variance equation $\langle\Psi_m|\hat{H}^2|\Psi_m\rangle = E_m^2$ [32, 39]. In the case of electronic systems ($\ell \equiv ijkl$) the Hamiltonian (1) is

$$\hat{H}_e = \sum_{ijkl} f_{ijkl}\,\hat{a}_i^\dagger \hat{a}_j^\dagger \hat{a}_l \hat{a}_k\,, \tag{3}$$

where $\hat{a}_i$ and $\hat{a}_i^\dagger$ are fermionic annihilation and creation operators, respectively, and the relevant many-body operators, $\hat{h}_\ell$, of equation (1) are two-particle terms only. Thus, the CSE (2) for the electronic problem becomes:

$$\langle\Psi_m|\hat{a}_i^\dagger \hat{a}_j^\dagger \hat{a}_l \hat{a}_k\left(\hat{H}_e - E_m\right)|\Psi_m\rangle = 0. \tag{4}$$

It is instructive to decompose the CSE (2) into two expectation values, containing an anti-commutator $\{\cdot,\cdot\}$ and a commutator $[\cdot,\cdot]$:

$$\langle\Psi_m|\left\{\hat{h}_\ell, \hat{H} - E_m\right\}|\Psi_m\rangle + \langle\Psi_m|\left[\hat{h}_\ell, \hat{H}\right]|\Psi_m\rangle = 0. \tag{5}$$

As described in several prior works for the electronic problem, this decomposition can be used to optimize a sequence of exponential (unitary and anti-unitary) ansätze that converge trial wave functions to the exact stationary states either through classical [40–47] or quantum [25, 26, 28, 29, 38, 48–50] computing methods. Furthermore, the simultaneous presence of anti-unitary and unitary operators makes the ansatz a very flexible one that can contain dissipative and non-dissipative terms [26]. Interestingly, while similar operator combinations are the focus of recent efforts in developing variational ansätze for ground-state preparation [51], they emerge naturally in the CSE framework.

Although the CSE is fully general, so far it has been barely used beyond the realm of electronic structure theory [28, 38]. We now apply the CSE framework to tackle the eigenstates of the Pauli-Fierz (PF) Hamiltonian.

*PF CSE*.— The nonrelativistic PF Hamiltonian describes the interaction of a molecular system with a cavity mode through the coupling of the electronic dipole moment to a bosonic field, and attempts to model the physics of, for example, electronic systems in mirrored cavities [52–55]. Many-body methods such as quantum electrodynamics Hartree–Fock (QED-HF), density functional theory

(QEDFT/QED-DFT) [56–61], and coupled cluster (QED-CC) [24, 62, 63] have been benchmarked on this approximate Hamiltonian. The PF Hamiltonian, in the length gauge with the dipole approximation [57, 64], is not in general restricted to a single bosonic mode; however, we will only consider the single-mode case as described by:

$$\hat{H}_{\mathrm{PF}} = \hat{H}_e + \omega \hat{b}^\dagger \hat{b} - \sqrt{\frac{\omega}{2}} (\lambda \cdot \hat{\mu}) \left(\hat{b}^\dagger + \hat{b}\right) + \frac{1}{2} (\lambda \cdot \hat{\mu})^2 , \tag{6}$$

where the first term, $\hat{H}_e$, is the traditional electronic Hamiltonian as seen in equation (3). The second term describes the energy of the cavity where $\omega$ is the fundamental frequency of the bosonic cavity mode and $\hat{b}$ and $\hat{b}^\dagger$ are the bosonic annihilation and creation operators, respectively. The third term depicts the coupling between the molecular dipole and the cavity where $\hat{\mu}$ is the molecular dipole moment, and $\lambda$ is the coupling vector. Finally, the last term is the dipole self-energy (DSE). An excellent introduction to QED-many-body methods and the coherent-state form of the PF Hamiltonian, used for construction of the Hartree–Fock reference state, can be found in reference [54].

The CSE for general mixed Fermi-Boson systems was derived by us in [38] and can be applied to the PF's ground state to generate the following set of CSEs:

$$\langle \Psi | \hat{\Gamma}^{ij}_{kl} \left(\hat{H}_{\mathrm{PF}} - E\right) | \Psi \rangle = 0 \tag{7a}$$

$$\langle \Psi | \hat{\Delta}^{i}_{j} \left(\hat{H}_{\mathrm{PF}} - E\right) | \Psi \rangle = 0 \tag{7b}$$

$$\langle \Psi | \hat{b}^\dagger \hat{b} \left(\hat{H}_{\mathrm{PF}} - E\right) | \Psi \rangle = 0, \tag{7c}$$

where $\hat{\Gamma}^{ij}_{kl} = \hat{a}^\dagger_i \hat{a}^\dagger_j \hat{a}_l \hat{a}_k$ and $\hat{\Delta}^{i}_{j} = (\hat{b}^\dagger + \hat{b}) \hat{a}^\dagger_i \hat{a}_j$ are, respectively, two-body fermionic and mixed (i.e. Fermi-Bose) density operators. We reiterate that, since the CSE has the same set of solutions as the Schrödinger equation, equations (7*a*) are satisfied by the exact ground state of the PF Hamiltonian. Furthermore, as explained in equation (5), the set of CSEs (7*a*) can be further decomposed into a Hermitian and an anti-Hermitian part, the latter comprising the following set of equations:

$$\langle \Psi | \left[\hat{\Gamma}^{ij}_{kl}, \hat{H}_{\mathrm{PF}}\right] | \Psi \rangle = 0 \tag{8a}$$

$$\langle \Psi | \left[\hat{\Delta}^{i}_{j}, \hat{H}_{\mathrm{PF}}\right] | \Psi \rangle = 0. \tag{8b}$$

The anti-Hermitian counterpart to equation (7*c*) vanishes and thus we do not consider it here. We call this anti-Hermitian subset of equations, the ACSE. Formally, the ACSE is not exact because it can be satisfied by a wave function that does not satisfy the CSE (or the Schrödinger equation) [41, 47]. Model spin systems in which the ACSE possesses spurious solutions are discussed in references [26, 47]. Practically, however, we find that the solution of the ACSE converges to the FCI wave function for molecules treated on noiseless quantum simulators [25, 26, 29, 48, 49]. Because of this agreement with FCI, we apply only the ACSE part of the CSE in the Results section.

*PF CQE.*— On modern quantum devices, the CQE algorithm measures the total residuals of equations (7*a*) for quantum states. Such a residual can then be used to guide a sequence of trial wave functions toward an *exact* eigenstate by iteratively applying a sequence of exponential transformations. Since our scheme is agnostic to the statistics of the system [26, 28, 29, 48–50], we apply it here to the PF Hamiltonian. To resolve its ground and excited states, we focus on a subset of the CQE algorithms, the ACSE, because it provides a simple and practical implementation on quantum hardware.

Our scheme is as follows: at iteration $(n+1)$ the wave function results from an exponential transformation of the wave function at iteration $(n)$ [38]:

$$|\Psi^{(n+1)}\rangle = \exp\left(\eta_B \hat{B}^{(n)}\right) \exp\left(\eta_A \hat{A}^{(n)}\right) |\Psi^{(n)}\rangle, \tag{9}$$

where

$$\hat{A}^{(n)} = \sum_{ik,jl} A^{(n)}_{ik,jl} \hat{\Gamma}^{ij}_{kl} \quad \text{and} \quad \hat{B}^{(n)} = \sum_{i,j} B^{(n)}_{ij} \hat{\Delta}^{i}_{j}. \tag{10}$$

Here $\hat{A}^{(n)}$ and $\hat{B}^{(n)}$ are the anti-Hermitian fermionic and mixed operators, respectively. The parameters $\eta_A$ and $\eta_B$ can be interpreted as learning rates of the algorithm and can be set equal to simplify the optimization procedure. Faster convergence, however, is achieved when both learning rates are optimized independently.

Notice that if the unitary $e^{\eta_A \hat{A}^{(n)}}$ is applied to a (normalized) wave function $|\Psi^{(n)}\rangle$, the total energy of the transformed state is (in leading order of $\eta_A$): $\mathcal{E}_{n+1} = \mathcal{E}_n + \eta_A \langle \Psi^{(n)} | [\hat{H}_{\rm PF}, \hat{A}^{(n)}] | \Psi^{(n)} \rangle + \mathcal{O}(\eta_A^2)$ where $\mathcal{E}_n = \langle \Psi^{(n)} | \hat{H}_{\rm PF} | \Psi^{(n)} \rangle$. As a result, the anti-Hermitian portion of the CSE, seen in equations (8*a*), can be used as a residual to find the optimal operator at each step, and the anti-Hermitian parameters can be updated as follows:

$$A^{(n)} = \langle \Psi^{(n)} | \left[ \hat{\Gamma}, \hat{H}_{\rm PF} \right] | \Psi^{(n)} \rangle \tag{11a}$$

$$B^{(n)} = \langle \Psi^{(n)} | \left[ \hat{\Delta}, \hat{H}_{\rm PF} \right] | \Psi^{(n)} \rangle. \tag{11b}$$

Measurement of the fermionic residual can be done through an approximate method that only requires the measurement of two-body operators, instead of the three-body operators needed for the exact residual, by measuring,

$$A^{(n)}_{ik,jl} = \frac{1}{2i\delta} \left( \langle +_n | \hat{\Gamma}^{ij}_{kl} | +_n \rangle - \langle -_n | \hat{\Gamma}^{ij}_{kl} | -_n \rangle \right) + \mathcal{O}\left(\delta^2\right) \tag{12}$$

where $|\pm_n\rangle = e^{\pm i\delta \hat{H}_{\rm PF}} |\Psi^{(n)}\rangle$ [25]. Tomography of the *exact* mixed particle residuals $B^{(n)}_{ij}$, on the other hand, only requires measurement of two-body fermionic operators. Thus the number of measurements for both the fermionic and mixed residuals scale as $\mathcal{O}(r^4)$, where $r$ is the number of orbitals. However, utilizing symmetries of the reduced density matrix as well as techniques like clique covering of Pauli words considerably lowers the scaling as many of the mixed residual terms qubit-wise commute with the fermionic terms [65].

It is worth emphasizing the key differences between our algorithm and VQE-based approaches, adapted to the many-body problem. ADAPT-VQE, for instance, iteratively builds a variational ansatz for the wave function by selecting from a predefined pool of operators [66]. The ansatz is often described as being a form of coupled cluster, but the stationarity condition of the ansatz does not produce the coupled cluster equations [35]. In fact, the ansatz is a subset of the ACSE ansatz with its stationarity generating a subset of the ACSE [40, 41]. The ADAPT-VQE algorithm's key feature is its operator selection process: (*i*) in each step the operator with the largest gradient is added to the left end of the ansatz, accompanied by a new variational parameter and (*ii*) all parameters are then re-optimized and the process is repeated until the gradient vector falls below a specified threshold $\varepsilon$ [66]. TETRIS-ADAPT-VQE, a recent improvement of the method, also includes at each step the operator with the largest gradient, that is not supported by the qubits already present in the ansatz [67].

The main differences of the ADAPT-VQE algorithm from the CQE are (1) its reliance upon a predefined pool of operators and (2) its reoptimization of all variational parameters at each iteration [25, 26, 28, 29, 48–50]. First, the CQE works with a potentially infinite pool of operators at each iteration with the pool being defined by the residual matrix of the CSE (or ACSE) [26, 29]. The CQE can either use the entire pool at each iteration or a more limited pool like the ADAPT-VQE, as in the recently proposed shadow CSE ansatz [68] inspired by shadow tomography. Second, unlike the ADAPT-VQE in which all parameters must be optimized to satisfy the global variational principle, the optimal operator in the CQE is selected at each iteration in the context of a *local* optimization method such that reoptimization of the parameters from previous iterations is unnecessary; e.g. in gradient descent, the optimal operator is the gradient of the CSE (or ACSE) ansatz [69]. The CQE is able to optimize only the parameters at a given iteration because such a local optimization in the CSE ansatz is sufficient to imply the CSE and hence, the Schrödinger equation at the minimum. [47, 70].

*Results*.— We first discuss the predicted results from the ACSE, QED-CC, and QED-FCI for the rectangular conformation of $H_4$, as it is distorted into and out of the square geometry. The coupled cluster methods are named such that QED-CCSD-*n* refers to coupled-cluster with single and double fermionic cluster terms combined with bosonic and mixed cluster terms containing up to *n* bosonic creation operators [24]. In line with this convention, we write ACSE-*n* and QED-FCI-*n* to refer to ACSE and QED-FCI methods that allow for up to *n* excitations in the bosonic degrees of freedom. Additionally, as the ACSE presented above is meant for quantum devices, we choose to use a variational classical-computing version of UCC with single and double excitations (UCCSD), the popular VQE ansatz [71], without truncating the Baker–Campbell–Hausdorff expansion of the exponential. After comparing these methods, we demonstrate the effectiveness of the ACSE algorithm on an IBM Quantum device for $H_2$ coupled to a bosonic bath. All results use the Slater-type orbital (STO-3G) basis set.

Figure 1 shows the ground and first excited-state energies for rectangular $H_4$ as the molecule is distorted into and out of its square conformation (or from the $D_{2h}$ symmetry group into the $D_{4h}$ group) at several different coupling strengths. The CC results in the figure 1(a) with $\lambda = 0.0$ show a cusp in the energy due to

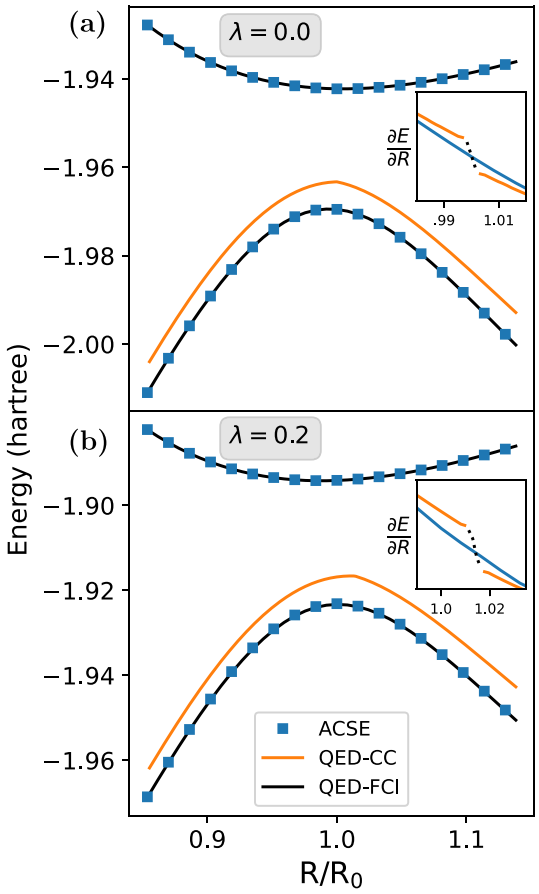


**Figure 1.** Comparison of energies from QED-CC and the ACSE in the deformation of rectangular $H_4$ coupled to a cavity mode. $R_0$ = 1.23 Å refers to the length of the constant $x$-axis of $H_4$, while R is the variable $z$-axis length. $\lambda$ refers to the coupling strength in the Pauli–Fierz Hamiltonian oriented along the $z$-axis. The embedded figures show the gradients of the potential energy surfaces produced by the ACSE and CC near the cusp. The level of theory for each method is ACSE-1, QED-CCSD-1, and QED-FCI-1.

the transition between the restricted Hartree–Fock (RHF) reference $A_gB_{3u}$ and $A_gB_{1u}$ conformations [72–75]; this cusp results in a discontinuity in the derivative of the potential energy surface for CC as seen in the embedded figure. The ACSE, however, starting from the same single-reference Hartree–Fock determinant, is able to resolve the energy to well below chemical accuracy and appropriately mix the different symmetry states. In particular, at the square conformation (the most difficult point to converge) the ACSE reaches chemical accuracy in 20 iterations. Additionally, the ACSE is able to recover the first excited state without any modification to the algorithm when given a singly excited configuration from the RHF reference state as an initial guess. We also find that simultaneously resolving the excited and ground states [27, 76] works well but requires an increased number of iterations to resolve both states to the same level of accuracy as a single-state method.

As the dipole coupling along the $z$-axis is increased, the energy of the $A_gB_{3u}$ determinant increases faster than the $A_gB_{1u}$ determinant's energy causing QED-HF to predict incorrectly a peak further into the compressed region. This effect arises because, while both determinants see an increase in energy due to a DSE term of equation (6), only the determinant aligned with the dipole moment ($A_gB_{1u}$) is able to reap the benefits of the energetically favorable exchange-like integral term that appears in the Hartree–Fock treatment of the DSE [54]. This shift in character makes QED-HF a poor initial guess for CC; therefore, the CC calculations are seeded with several reference states of different symmetries, with the lowest resulting energy kept for the figure. The CC results are still fairly inaccurate, and now the peak of the CC energy is shifted away from the FCI peak energy. Additionally, the cusp occurs after the peak energy for coupled cluster and is shifted further into the elongated region ($R > R_0$), as can be seen in the embedded figure. The ACSE, on the other hand, captures better-than-chemically-accurate results regardless of the coupling strength for both the ground and excited states, resolving the square conformation to chemical accuracy in $\approx 80$ iterations. This demonstrates the ACSE's ability to treat static correlation and handle strong cavity effects correctly.

Figure 2 shows the frontier (highest and lowest) natural orbital occupations (HONO and LUNO, respectively) for $H_4$ as the molecule is deformed. The results in the no-coupling limit demonstrate the

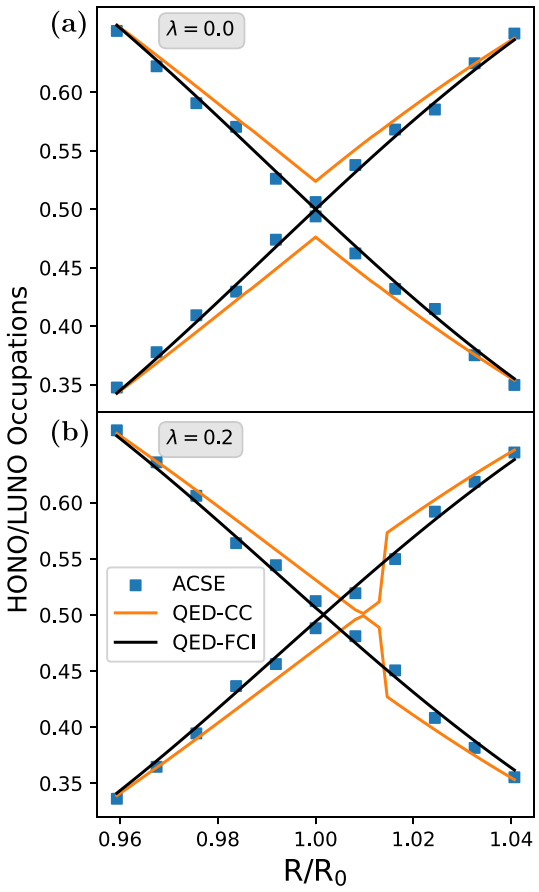


**Figure 2.** HONO and LUNO orbital occupations from QED-CC and the ACSE in the deformation of $H_4$ coupled to a cavity mode. $R_0 = 1.23$ Å refers to the length of the constant $x$-axis of $H_4$, while $R$ is the variable $z$-axis length. $\lambda$ refers to the coupling strength in the Pauli-Fierz Hamiltonian oriented along the $z$-axis. The level of theory for each method is ACSE-1, QED-CCSD-1, and QED-FCI-1.

single-reference limitations of coupled cluster which is unable to predict the orbital degeneracy. The ACSE, as expected from the highly accurate energy curves, is able to properly mix the two determinants. In the strongly coupled region, we begin to see the cause of the shifted peak in figure 1. In fact, the coupling makes it energetically possible for CC to retain the $A_g B_{3u}$ configuration until after the orbital degeneracy where the energy peaks. This degeneracy is predicted after the actual FCI orbital degeneracy as first reported by Paldus [73]. The CC result then spontaneously jumps to the $A_g B_{1u}$ configuration causing the discontinuity seen in the energy. Thus the coupling is able to separate the orbital degeneracy from the configurational degeneracy that frustrates single-reference CC methods.

Finally, figure 3 shows the dissociation curve of $H_2$ when it is strongly coupled to a bosonic bath (i.e. $\lambda = .2$). The ACSE results are obtained on the 127-qubit `ibm_cleveland` device which uses the Eagle r3 processor. The system is mapped to three qubits; two of these qubits model the fermionic degrees of freedom in the CI STO-3G basis using the $2^2 = 4$ configurations for a binary mapping, while the final qubit is devoted to modeling a truncated bosonic bath using a binary mapping for the zero and one population states. Utilizing the Qiskit estimator function for obtaining density matrix elements, we are able to take advantage of the built-in zero noise extrapolation, gate/measurement twirling, and clique covering algorithms [77]. The result is a significant increase in accuracy from QED-HF, with a mean absolute error of ≈11 millihartrees from QED-FCI-1. Additionally, the ACSE is able to obtain these energies in fewer than five iterations from the QED-HF reference state, demonstrating that the unitary ACSE ansatz is a practical algorithm for resolving polaritonic ground states on NISQ hardware.

*Conclusions.*— In conclusion, we have presented a novel polaritonic contracted quantum eigensolver capable of resolving eigenstates of cavity-modified systems, even in the presence of strong correlations. Our approach employs an iterative unitary ansatz derived from the contracted Schrödinger equation that can be implemented on modern quantum devices. Its high accuracy is demonstrated by its numerical performance when modeling the PF Hamiltonian on the deformed rectangular $H_4$ coupled to a cavity mode, and its current feasibility on NISQ hardware is showcased by computing the dissociation curve of $H_2$ strongly

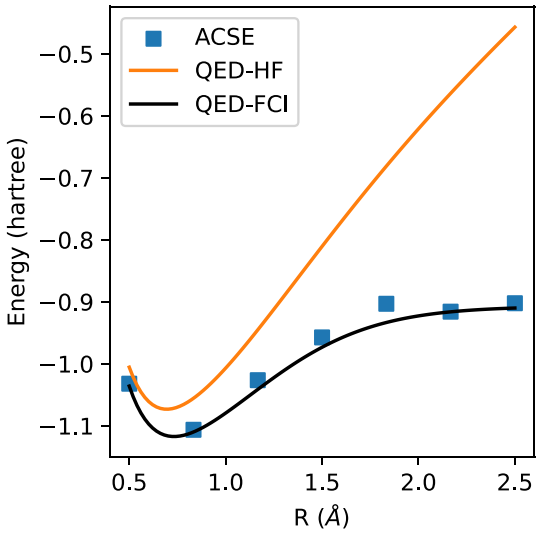


**Figure 3.** Dissociation curve of $H_2$ coupled to a bosonic bath on an IBM quantum device. The coupling strength was set to $\lambda = .2$. Measurement was performed on `ibm_cleveland` using 4096 shot per circuit. The level of theory for each method is ACSE-1 and QED-FCI-1.

coupled to a bosonic bath. The results of this research reveal the broad applicability of CQEs and their striking agnostic statistical nature, which ensures their applicability to arbitrary quantum systems.

These developments suggest many interesting research directions. Leveraging the ACSE's accurate treatment of multi-reference character, more physically realistic multimode PF Hamiltonians could be investigated as these extra degrees of freedom can drastically change the behavior of the system [13, 78]. Additionally, the ACSE has been shown to resolve conical intersections [79], so it could easily be extended to discover cavity-induced conical intersections, a promising avenue for novel synthetic chemistry [23, 24, 80, 81]. As the ACSE accurately predicts energies in both the weak and strong coupling regimes, it could also be utilized to study the ultra-high coupling regimes found in nanoplasmonic systems like picocavities that are used for manipulating intramolecular bonds [82, 83]. Finally, the ACSE's adept handling of bosonic statistics could be employed on the study of dipolar or mixtures of Bose gases, where fascinating states of matter can emerge, such as supersolidity [84].

## Data availability statement

All data that support the findings of this study are included within the article (and any supplementary files).

## Acknowledgment

D A M gratefully acknowledges the U S National Science Foundation Grant No. CHE-2155082 and the U.S. Department of Energy, Office of Basic Energy Sciences, Grant DE-SC0019215. C L B -R gratefully acknowledges financial support from the Royal Society of Chemistry and the European Union's Horizon Europe Research and Innovation program under the Marie Skłodowska-Curie Grant Agreement n°101065295–RDMFTforbosons. Views and opinions expressed are however those of the author only and do not necessarily reflect those of the European Union or the European Research Executive Agency. We acknowledge the use of IBM Quantum services for this work. The views expressed are those of the authors and do not reflect the official policy or position of IBM or the IBM Quantum team.

## Code availability

All code will be made available upon reasonable request.

## Author contributions

S W, Y W, C L B-R, and D A M conceived of the Project, interpreted the results, and wrote the manuscript. S W wrote the code and performed the computations including calculations on an IBM quantum computer.

## ORCID iDs

Samuel Warren https://orcid.org/0000-0001-5713-4454
Yuchen Wang https://orcid.org/0000-0003-0479-3776
Carlos L Benavides-Riveros https://orcid.org/0000-0001-6924-727X
David A Mazziotti https://orcid.org/0000-0002-9938-3886

## References

[1] Hertzog M, Wang M, Mony J and Börjesson K 2019 Strong light–matter interactions: a new direction within chemistry *Chem. Soc. Rev.* **48** 937
[2] Fregoni J, Garcia-Vidal F J and Feist J 2022 Theoretical challenges in polaritonic chemistry *ACS Photon.* **9** 1096
[3] Ruggenthaler M, Sidler D and Rubio A 2023 Understanding polaritonic chemistry from ab initio quantum electrodynamics *Chem. Rev.* **123** 11191
[4] Schwartz T, Hutchison J A, Genet C and Ebbesen T 2011 Reversible switching of ultrastrong light-molecule coupling *Phys. Rev. Lett.* **106** 196405
[5] Kowalewski M, Bennett K and Mukamel S 2016 Cavity femtochemistry: manipulating nonadiabatic dynamics at avoided crossings *J. Phys. Chem. Lett.* **7** 2050
[6] Berghuis A, Halpin A, Le-Van Q, Ramezani M, Wang S, Murai S and Gómez Rivas J 2019 Enhanced delayed fluorescence in tetracene crystals by strong light-matter coupling *Adv. Funct. Mater.* **29** 1901317
[7] Mauro L, Caicedo K, Jonusauskas G and Avriller R 2021 Charge-transfer chemical reactions in nanofluidic Fabry-Pérot cavities *Phys. Rev.* B **103** 165412
[8] Mandal A and Huo P 2019 Investigating new reactivities enabled by polariton photochemistry *J. Phys. Chem. Lett.* **10** 5519
[9] Forn-Díaz P, Lamata L, Rico E, Kono J and Solano E 2019 Ultrastrong coupling regimes of light-matter interaction *Rev. Mod. Phys.* **91** 025005
[10] Beltrán-Romero S, Rodríguez F J, Quiroga L and Johnson N 2023 Cavity-induced switching between Bell-state textures in a quantum dot *Phys. Rev.* B **108** 195409
[11] Schlawin F, Kennes D and Sentef M 2022 Cavity quantum materials *Appl. Phys. Rev.* **9** 011312
[12] Bloch J, Cavalleri A, Galitski V, Hafezi M and Rubio A 2022 Strongly correlated electron–photon systems *Nature* **606** 41
[13] Buchholz F, Theophilou I, Giesbertz K J H, Ruggenthaler M and Rubio A 2020 Light–matter hybrid-orbital-based first-principles methods: the influence of polariton statistics *J. Chem. Theory Comput.* **16** 5601
[14] Lanyon B *et al* 2010 Towards quantum chemistry on a quantum computer *Nat. Chem.* **2** 106
[15] Barkoutsos P *et al* 2018 Quantum algorithms for electronic structure calculations: particle-hole hamiltonian and optimized wave-function expansions *Phys. Rev.* A **98** 022322
[16] Callison A and Chancellor N 2022 Hybrid quantum-classical algorithms in the noisy intermediate-scale quantum era and beyond *Phys. Rev.* A **106** 010101
[17] Anand A, Schleich P, Alperin-Lea S, Jensen P, Sim S, Díaz-Tinoco M, Kottmann J, Degroote M, Izmaylov A and Aspuru-Guzik A 2022 A quantum computing view on unitary coupled cluster theory *Chem. Soc. Rev.* **51** 1659
[18] Chan G, Kállay M and Gauss J 2004 State-of-the-art density matrix renormalization group and coupled cluster theory studies of the nitrogen binding curve *J. Chem. Phys.* **121** 6110
[19] Van Voorhis T and Head-Gordon M 2000 Benchmark variational coupled cluster doubles results *J. Chem. Phys.* **113** 8873
[20] Pavošević F and Flick J 2021 Polaritonic unitary coupled cluster for quantum computations *J. Phys. Chem. Lett.* **12** 9100
[21] Benavides-Riveros C L, Lathiotakis N N and Marques M A L 2017 Towards a formal definition of static and dynamic electronic correlations *Phys. Chem. Chem. Phys.* **19** 12655
[22] Grimsley H, Claudino D, Economou S, Barnes E and Mayhall N 2020 Is the trotterized UCCSD ansatz chemically well-defined? *J. Chem. Theory Comput.* **16** 1–6
[23] Mordovina U, Bungey C, Appel H, Knowles P J, Rubio A and Manby F R 2020 Polaritonic coupled-cluster theory *Phys. Rev. Res.* **2** 023262
[24] Haugland T S, Ronca E, Kjønstad E F, Rubio A and Koch H 2020 Coupled cluster theory for molecular polaritons: changing ground and excited states *Phys. Rev.* X **10** 041043
[25] Smart S E and Mazziotti D A 2021 Quantum solver of contracted eigenvalue equations for scalable molecular simulations on quantum computing devices *Phys. Rev. Lett.* **126** 070504
[26] Smart S E and Mazziotti D A 2024 Verifiably exact solution of the electronic Schrödinger equation on quantum devices *Phys. Rev.* A **109** 022802
[27] Benavides-Riveros C L, Wang Y, Warren S and Mazziotti D 2024 Quantum simulation of excited states from parallel contracted quantum eigensolvers *New J. Phys.* **26** 033020
[28] Wang Y, Smith L M and Mazziotti D A 2023 Quantum simulation of bosons with the contracted quantum eigensolver *New J. Phys.* **25** 103005
[29] Smart S, Boyn J and Mazziotti D 2022 Resolving correlated states of benzyne with an error-mitigated contracted quantum eigensolver *Phys. Rev.* A **105** 022405
[30] Nakatsuji H 1976 Equation for the direct determination of the density matrix *Phys. Rev.* A **14** 41
[31] Cohen L and Frishberg C 1976 Hierarchy equations for reduced density matrices *Phys. Rev.* A **13** 927
[32] Mazziotti D A 1998 Contracted Schrödinger equation: Determining quantum energies and two-particle density matrices without wave functions *Phys. Rev.* A **57** 4219
[33] Colmenero F and Valdemoro C 1993 Approximating q-order reduced density matrices in terms of the lower-order ones. II. Applications *Phys. Rev.* A **47** 979
[34] Nakatsuji H and Yasuda K 1996 Direct determination of the quantum-mechanical density matrix using the density equation *Phys. Rev. Lett.* **76** 1039
[35] Mazziotti D A 1999 Comparison of contracted Schrödinger and coupled-cluster theories *Phys. Rev.* A **60** 4396
[36] Mukherjee D and Kutzelnigg W 2001 Irreducible Brillouin conditions and contracted Schrödinger equations for n-electron systems. I. The equations satisfied by the density cumulants *J. Chem. Phys.* **114** 2047

[37] Yasuda K 2002 Uniqueness of the solution of the contracted Schrödinger equation *Phys. Rev.* A **65** 052121
[38] Warren S, Wang Y, Benavides-Riveros C L and Mazziotti D A 2024 Exact ansatz of fermion-boson systems for a quantum device *Phys. Rev. Lett.* **133** 080202
[39] Mazziotti D 2007 *Contracted Schrödinger equation, in Reduced Density Matrix Mechanics: With Application to many Electron Atoms and Molecules* vol 8 (Wiley) Ch. chapter, pp 165–203
[40] Mazziotti D A 2006 Anti-Hermitian contracted Schrödinger equation: Direct determination of the two-electron reduced density matrices of many-electron molecules *Phys. Rev. Lett.* **97** 143002
[41] Mazziotti D A 2007 Anti-Hermitian part of the contracted Schrödinger equation for the direct calculation of two-electron reduced density matrices *Phys. Rev.* A **75** 022505
[42] Mazziotti D A 2007 Multireference many-electron correlation energies from two-electron reduced density matrices computed by solving the anti-Hermitian contracted Schrödinger equation *Phys. Rev.* A **76** 052502
[43] Snyder J W and Mazziotti D A 2011 Photoexcited conversion of gauche-1,3-butadiene to bicyclobutane via a conical intersection: Energies and reduced density matrices from the anti-Hermitian contracted Schrödinger equation *J. Chem. Phys.* **135** 024107
[44] Gidofalvi G and Mazziotti D A 2009 Direct calculation of excited-state electronic energies and two-electron reduced density matrices from the anti-Hermitian contracted Schrödinger equation *Phys. Rev.* A **80** 022507
[45] Alcoba D R, Valdemoro C, Tel L M, Pérez-Romero E and Ona O B 2011 Optimized solution procedure of the *G*-particle-hole hypervirial equation for multiplets: application to doublet and triplet states *J. Phys. Chem.* A **115** 2599
[46] Boyn J-N and Mazziotti D A 2021 Accurate singlet–triplet gaps in biradicals via the spin averaged anti-Hermitian contracted Schrödinger equation *J. Chem. Phys.* **154** 134103
[47] Mazziotti D A 2004 Exactness of wave functions from two-body exponential transformations in many-body quantum theory *Phys. Rev.* A **69** 012507
[48] Boyn J-N, Lykhin A O, Smart S E, Gagliardi L and Mazziotti D A 2021 Quantum-classical hybrid algorithm for the simulation of all-electron correlation *J. Chem. Phys.* **155** 244106
[49] Smart S E and Mazziotti D A 2022 Many-fermion simulation from the contracted quantum eigensolver without fermionic encoding of the wave function *Phys. Rev.* A **105** 062424
[50] Wang Y and Mazziotti D A 2023 Electronic excited states from a variance-based contracted quantum eigensolver *Phys. Rev.* A **108** 022814
[51] Cobos J, Locher D, Bermudez A, Müller M and Rico E 2024 Noise-aware variational eigensolvers: a dissipative route for lattice gauge theories *PRX Quantum* **5** 030340
[52] Spohn H 2004 *Dynamics of Charged Particles and Their Radiation Field* (Cambridge: Cambridge University Press)
[53] Mandal A, Taylor M, Weight B, Koessler E, Li X and Huo P 2023 Theoretical advances in polariton chemistry and molecular cavity quantum electrodynamics *Chem. Rev.* **123** 9786
[54] Foley IV J., McTague J., and DePrince III A., Ab initio methods for polariton chemistry, Chem. Phys. Rev. **4** 041301 (2023)
[55] Mukhopadhyay P, Stetina T and Wiebe N 2024 Quantum simulation of the first-quantized Pauli-Fierz Hamiltonian *PRX Quantum* **5** 010345
[56] Ruggenthaler M, Mackenroth F and Bauer D 2011 Time-dependent Kohn-Sham approach to quantum electrodynamics *Phys. Rev.* A **84** 042107
[57] Tokatly I V 2013 Time-dependent density functional theory for many-electron systems interacting with cavity photons *Phys. Rev. Lett.* **110** 233001
[58] Ruggenthaler M, Flick J, Pellegrini C, Appel H, Tokatly I and Rubio A 2014 Quantum-electrodynamical density-functional theory: bridging quantum optics and electronic-structure theory *Phys. Rev.* A **90** 012508
[59] Vu N, McLeod G, Hanson K and DePrince III A 2022 Enhanced diastereocontrol via strong light–matter interactions in anoptical cavity *J. Phys. Chem.* A **126** 9303
[60] Pavošević F and Rubio A 2022 Wavefunction embedding for molecular polaritons *J. Chem. Phys.* **157** 094101
[61] Liebenthal M, Vu N and DePrince III A 2023 Assessing the effects of orbital relaxation and the coherent-state transformation in quantum electrodynamics density functional andcoupled-cluster theories *J. Phys. Chem.* A **127** 5264
[62] Haugland T, Schäfer C, Ronca E, Rubio A and Koch H 2021 Intermolecular interactions in optical cavities: an ab initio QED study *J. Chem. Phys.* **154** 094113
[63] Liebenthal M, Vu N and DePrince III A 2022 Equation-of-motion cavity quantum electrodynamics coupled-cluster theory for electron attachment *J. Chem. Phys.* **156** 054105
[64] Babiker M, Loudon R and Series G W 1983 Derivation of the power-Zienau-Woolley Hamiltonian in quantum electrodynamics by gauge transformation *Proc. R. Soc. Lond.* A **385** 439
[65] Verteletskyi V, Yen T and Izmaylov A F 2020 Measurement optimization in the variational quantum eigensolver using a minimum clique cover *J. Chem. Phys.* **152** 124114
[66] Grimsley H R, Economou S, Barnes E and Mayhall N 2019 An adaptive variational algorithm for exact molecular simulations on a quantum computer *Nat. Comm.* **10** 3007
[67] Anastasiou P, Chen Y, Mayhall N, Barnes E and Economou S 2024 Tetris-adapt-vqe: an adaptive algorithm that yields shallower, denser circuit ansätze *Phys. Rev. Res.* **6** 013254
[68] Wang Y, Avdic I and Mazziotti D A,2024 Shadow ansatz for the many-fermion wave function in scalable molecular simulations on quantum computing devices (arXiv2408.11026)
[69] Smart S E and Mazziotti D A 2022 Accelerated convergence of contracted quantum eigensolvers through a quasi-second-order, locally parameterized optimization *J. Chem. Theory Comput.* **18** 5286–96
[70] Mazziotti D A 2020 Exact two-body expansion of the many-particle wave function *Phys. Rev.* A **102** 030802
[71] Harsha G, Shiozaki T and Scuseria G 2018 On the difference between variational and unitary coupled cluster theories *J. Chem. Phys.* **148** 044107
[72] Jankowski K and Paldus J 1980 Applicability of coupled-pair theories to quasi degenerate electronic states: a model study *Int. J. Quantum Chem.* **18** 1243
[73] Paldus J, Piecuch P, Pylypow L and Jeziorski B 1993 Application of Hilbert-space coupled-cluster theory to simple $(H_2)_2$ model systems: planar models *Phys. Rev.* A **47** 2738
[74] Marie A, Kossoski F and Loos P-F 2021 Variational coupled cluster for ground and excited states *J. Chem. Phys.* **155** 104105
[75] Robinson J and Knowles P 2012 Benchmark quasi-variational coupled cluster calculations of multiple bond breaking *J. Chem. Theory Comput.* **8** 2653

[76] Benavides-Riveros C L, Chen L, Schilling C, Mantilla S and Pittalis S 2022 Excitations of quantum many-body systems via purified ensembles: a unitary-coupled-cluster-based approach *Phys. Rev. Lett.* **129** 066401
[77] Javadi-Abhari A, Treinish M Krsulich K Wood C Lishman J Gacon J Martiel S Nation P Bishop L S Cross A Johnson B and Gambetta J Quantum computing with Qiskit 2024 (arXiv: 2405.08810[quant-ph])
[78] Fischer E and Saalfrank P 2022 Cavity-induced non-adiabatic dynamics and spectroscopy of molecular rovibrational polaritons studied by multi-mode quantum models *J. Chem. Phys.* **157** 034305
[79] Wang Y and Mazziotti D A 2024 Quantum simulation of conical intersections *Phys. Chem. Chem. Phys.* **26** 11491
[80] Demekhin P and Cederbaum L 2013 Light-induced conical intersections in polyatomic molecules: general theory, strategies of exploitation and application *J. Chem. Phys.* **139** 154314
[81] Fábri C, Halász G and Vibók A 2022 Probing light-induced conical intersections by monitoring multidimensional polaritonic surfaces *J. Phys. Chem. Lett.* **13** 1172
[82] Flick J, Rivera N and Narang P 2018 Strong light-matter coupling in quantum chemistry and quantum photonics *Nanophotonics* **7** 1479
[83] Cortés E, Besteiro L, Alabastri A, Baldi A, Tagliabue G, Demetriadou A and Narang P 2020 Challenges in plasmonic catalysis *ACS Nano* **14** 16202
[84] Recati A and Stringari S 2023 Supersolidity in ultracold dipolar gases *Nat. Rev. Phys.* **5** 735